Chem Biol Drug Des 2012; **80:** 763–770

Research Article

doi: 10.1111/cbdd.12014

Modulation of Opioid Receptor Ligand Affinity and Efficacy Using Active and Inactive State Receptor Models

Jessica P. Anand[1], Lauren C. Purington[2,†], Irina D. Pogozheva[1], John R. Traynor[2,3] and Henry I. Mosberg[1,*]

[1]*Department of Medicinal Chemistry, College of Pharmacy, University of Michigan, 428 Church Street, Ann Arbor, MI 48109, USA*

[2]*Department of Pharmacology, Medical School, University of Michigan, Ann Arbor, MI 48109, USA*

[3]*Substance Abuse Research Center, University of Michigan, Ann Arbor, MI 48109, USA*

**Corresponding author: Henry I. Mosberg, him@umich.edu*

[†]*Current Address: Department of Pharmaceutical Sciences, Albany College of Pharmacy and Health Sciences, Albany, NY 12208, USA.*

Mu opioid receptor (MOR) agonists are widely used for the treatment of pain; however, chronic use results in the development of tolerance and dependence. It has been demonstrated that coadministration of a MOR agonist with a delta opioid receptor (DOR) antagonist maintains the analgesia associated with MOR agonists, but with reduced negative side-effects. Using our newly refined opioid receptor models for structure-based ligand design, we have synthesized several pentapeptides with tailored affinity and efficacy profiles. In particular, we have obtained pentapeptides 8, Tyr-c(S-S)[DCys-1Nal-Nle-Cys]NH_2, and 12, Tyr-c(S-S)[DCys-1Nal-Nle-Cys]OH, which demonstrates high affinity and full agonist behavior at MOR, high affinity but very low efficacy for DOR, and minimal affinity for the kappa opioid receptor (KOR). Functional properties of these peptides as MOR agonists/DOR antagonists lacking undesired KOR activity make them promising candidates for future *in vivo* studies of MOR/DOR interactions. Subtle structural variation of 12, by substituting D-Cys[5] for L-Cys[5], generated analog 13, which maintains low nanomolar MOR and DOR affinity, but which displays no efficacy at either receptor. These results demonstrate the power and utility of accurate receptor models for structure-based ligand design, as well as the profound sensitivity of ligand function on its structure.

Key words: delta opioid receptor, G protein-coupled receptors, mixed efficacy ligand, mu opioid receptor, opioid, peptide, structure-based design

Received 10 May 2012, revised 22 July 2012 and accepted for publication 2 August 2012

The recognition that a specific receptor often plays a pivotal role in a disease state shifted the drug discovery paradigm toward a 'one disease, one target' approach. The driving force behind this shift was the idea that the more specific a drug, the fewer negative side-effects it will elicit. Recently, however, it has been recognized that the simultaneous modulation of multiple targets may generate a more desirable drug profile, in some cases even reducing the development of negative side-effects (1,2). This concept is illustrated in the field of opioid analgesics, where the coadministration of a mu opioid receptor (MOR) agonist with a delta opioid receptor (DOR) antagonist provides all the expected analgesia of a MOR agonist, but with reduced negative side-effects, such as constipation and respiratory depression, and more interestingly, reduced tolerance and dependence liabilities (3–7), features that limit the clinical use of opioid analgesics (8).

Our laboratory and others (6–18) have explored the development of mixed efficacy ligands where MOR agonist activity is combined with DOR antagonism in the same molecule using a 'merged' pharmacophore (2). Such a multifunctional ligand would possess considerable advantages over the traditional approach of using a combination of selective opioid drugs with possibly differing pharmacokinetic or pharmacodynamic properties. Peptides provide a convenient starting point for the development of multifunctional opioid ligands. Many endogenous and synthetic opioid peptide ligands have been studied and their SAR has been well characterized, providing the foundation for applying rational design to existing structures to explore the MOR and DOR binding pockets.

Previous work in our laboratory resulted in lead peptide **1** (Tyr-c(S-S)[DCys-Phe-Phe-Cys]NH_2) (19), which displays full agonism at MOR and slightly reduced efficacy at DOR as well as high affinity for both receptors (Table 1). Because **1** has appreciable DOR efficacy, we then focused our efforts on designing ligands that retain MOR agonist activity, but with reduced DOR efficacy (6). Using our receptor models for both active and inactive states of MOR and DOR (6,8,20–24), we predicted that adding bulky aromatic substituents in the third or fourth position of peptide **1** would produce a steric clash in the DOR active state binding site, which would not be seen in the DOR inactive site, thus favoring binding to the DOR inactive state and consequently resulting in lower DOR efficacy (6). Docking to corresponding active and inactive state MOR

Table 1: Binding Affinities and Efficacies of Peptides **1**–**5**

		K_i (nM)			Efficacy (% standard)		
Peptide	Sequence	MOR	DOR	KOR	MOR	DOR	KOR
1	Tyr-c(S-S)[DCys-Phe-Phe-Cys]NH_2	0.27 ± 0.2	0.8 ± 0.3	8.6 ± 0.5	77 ± 9	69 ± 1.6	74 ± 17
2	Tyr-c(S-S)[DCys-Phe-Leu-Cys]NH_2	1.3 ± 0.7	2.0 ± 0.8	3100 ± 890	100 ± 2	74 ± 13	dns
3	Tyr-c(S-S)[DCys-Phe-Ile-Cys]NH_2	1.5 ± 0.7	0.3 ± 0.2	980 ± 310	93 ± 4	86 ± 7	dns
4	Tyr-c(S-S)[DCys-Phe-Nle-Cys]NH_2	1.6 ± 0.1	1.7 ± 0.3	2600 ± 130	104 ± 10	103 ± 1.5	nt
5	Tyr-c(S-S)[DCys-Phe-Nle-DCys]NH_2	0.62 ± 0.1	1.3 ± 0.4	210 ± 230	64 ± 6	47 ± 9.3	nt

Binding affinities (K_i) were obtained by competitive displacement of radiolabeled [^{3}H] diprenorphine. Efficacy data were obtained using [^{35}S] GTPγS binding assay. Efficacy is represented as per cent maximal stimulation relative to standard agonists DAMGO (MOR), DPDPE (DOR), or U69,593 (KOR) at 10 μM concentrations. All values are expressed as mean ± SEM of three separate assays performed in duplicate. Cyclization abbreviated as S-S for disulfide linkage, nt = not tested, dns = does not stimulate.

models revealed no analogous receptor state-specific adverse interactions; we therefore predicted that increasing steric bulk at position 3 or 4 would provide the desired MOR agonist/DOR antagonist profile. Incorporation of 1-Nal (1-naphthylalanine) or 2-Nal (2-naphthylalanine) into position 3 or 4 of **1** did indeed yield analogs with high MOR/low DOR efficacy, but all analogs also retained high KOR affinity (6). Such KOR activity is less desirable; while KOR agonists are known to provide some analgesic properties, they are also known to cause dysphoria, which severely limits their usefulness (25). This study makes further use of our receptor–ligand models to design analogs that maintain high affinity for both MOR and DOR, but not KOR, and display full MOR agonism and DOR antagonism.

Methods and Materials

Materials

All reagents and solvents were purchased from commercial sources and used without further purification. All chemicals and biochemicals were purchased from Sigma Aldrich (St. Louis, MO, USA) or Fisher Scientific (Hudson, NH, USA), unless otherwise noted. All tissue culture reagents were purchased from Gibco Life Sciences (Grand Island, NY, USA). Radioactive compounds were purchased from Perkin-Elmer (Waltham, MA, USA). Peptide synthesis reagents, amino acids, and Rink resin were purchased from Advanced Chem Tech (Louisville, KY, USA). Wang resins were purchased from Nova Biochem, EMD (Gibbstown, NJ, USA).

Solid-phase peptide synthesis

Peptides were synthesized using standard solid-phase Fmoc (fluorenylmethyloxycarbonyl) chemistry on a CS Bio CS336X Peptide Synthesizer (CS Bio Company, Menlo Park, CA, USA), using previously described protocols (26). C-terminal amide peptides were synthesized using Rink resin, C-terminal acid peptides were synthesized using Fmoc–Wang resin preloaded with the C-terminal amino acid. A 20% solution of piperidine in *N*-methyl-2-pyrrolidone (NMP) was used to remove the first Fmoc-protecting group before synthesis and again to remove the Fmoc-protecting group after each coupling cycle. Coupling was performed using a fourfold excess of amino acid and a solution of 0.4 M hydroxybenzotriazole (HOBt) and O-benzotriazole-N, N, N′, N′-tetramethyl-uroniumhexafluoro-phosphate (HBTU) in dimethylformamide (DMF), in the presence of diisopropylethylamine (DIEA). After the synthesis was complete, the resin was washed with NMP, then with dichloromethane, and dried under vacuum. The peptides were cleaved from the resin and side-chain-protecting groups removed by treatment at room temperature for 2 h with a cleavage cocktail consisting of 9.5 mL trifluoroacetic (TFA) acid, 0.25 mL triisopropylsilane (TIS), and 0.25 mL H_2O. The solution was concentrated *in vacuo*, and peptides were precipitated using cold, fresh diethylether. The filtered crude material was then purified using a Waters semipreparative HPLC (Waters Corporation, Milford, MA, USA) with a Vydac Protein and Peptide C18 column, using a linear gradient 10% solvent B (0.1% TFA acid in acetonitrile) in solvent A (0.1% TFA acid in water) to 60% solvent B in solvent A, at a rate of 1% per minute. The identity of all peptides were determined using ESI-MS performed on an Agilent Technologies LC/MS system using a 1200 Series LC and 6130 Quadrupole LC/MS (Agilent Technologies, Santa Clara, CA, USA) in positive mode with 50–100 μL injection volume and a linear gradient of 0% solvent D (0.02% TFA and 0.1% acetic acid (AcOH) in acetonitrile) in solvent C (0.02% TFA and 0.1% AcOH in water) to 60% solvent D in solvent C in 15 min. The purity of all peptides was determined using a Waters Alliance 2690 Analytical HPLC (Waters Corporation) and Vydac Protein and Peptide C18 reverse phase column, using a linear gradient of 0–70% solvent B in solvent A at a rate of 1% per minute. Linear peptides were purified to ≥95% purity by UV absorbance at 230 nm.

Disulfide cyclization of linear peptides

Pure linear disulfhydryl-containing peptide was dissolved at 1mg/mL in argon saturated solution of 1% (v/v) AcOH in H_2O at 4C. The pH of the peptide solution was raised to 8.5 using NH_4OH, followed by the addition of 4 molar equivalents of $K_3Fe(CN)_6$. The reaction mixture was stirred on ice, under argon for two minutes and quenched by addition of glacial acetic acid to pH 3.5. The reaction mixture was incubated with 100–200 mesh anion exchange resin AG-3-X4 (Biorad, Hercules, CA, USA) and swirled occasionally at room temperature until the solution was colorless. The crude mixture was then filtered, concentrated *in vacuo,* and purified to ≥98% purity as determined by UV absorbance at 230 nm as described earlier to yield the disulfide linked

cyclized peptides. The identity of cyclic peptides was determined by ESI-MS as described earlier.

Dithioether cyclization of linear peptides

A DMF solution of the linear peptide (15 mg/40 mL) containing 5 molar equivalents of 1,2-dibromoethane was added dropwise to a round-bottom flask containing 10 molar equivalents of potassium tert-butoxide in 100 mL of anhydrous DMF saturated with argon, on ice. The reaction was stirred for 2 h under argon, on ice, and then quenched to pH 3.5 with glacial acetic acid. Solvents were removed *in vacuo*, and the residue was purified to ≥98% purity as determined by UV absorbance at 230 nm as described earlier to afford the alkyl dithioether cyclized peptide. The identity of cyclic peptides was determined by ESI-MS as described earlier.

Cell lines and membrane preparations

C6-rat glioma cells stably transfected with a rat μ (C6-MOR) or rat δ (C6-DOR) opioid receptor (27) and Chinese hamster ovary (CHO) cells stably expressing a human κ (CHO-KOR) opioid receptor (28) were used for all *in vitro* assays. Cells were grown to confluence at 37 °C in 5% CO_2 in Dulbecco's modified Eagle's medium containing 10% fetal bovine serum and 5% penicillin/streptomycin. Membranes were prepared by washing confluent cells three times with ice-cold phosphate-buffered saline (0.9% NaCl, 0.61 mM Na_2HPO_4, 0.38 mM KH_2PO_4, pH 7.4). Cells were detached from the plates by incubation in warm harvesting buffer (20 mM HEPES, 150 mM NaCl, 0.68 mM EDTA, pH 7.4) and pelleted by centrifugation at 200 × *g* for 3 min. The cell pellet was suspended in ice-cold 50 mM Tris-HCl buffer, pH 7.4 and homogenized with a Tissue Tearor (Biospec Products, Inc, Bartlesville, OK, USA) for 20 s at setting 4. The homogenate was centrifuged at 20 000 × *g* for 20 min at 4 °C, and the pellet was rehomogenized in 50 mM Tris-HCl with a Tissue Tearor for 10 s at setting 2, followed by recentrifugation. The final pellet was resuspended in 50 mM Tris-HCl and frozen in aliquots at −80 °C. Protein concentration was determined via Bradford assay using bovine serum albumin as the standard.

Radioligand binding assays

Opioid ligand-binding assays were performed using competitive displacement of 0.2 nM [^{3}H]diprenorphine (250 μCi, 1.85TBq/mmol) by the test compound from membrane preparations containing opioid receptors. The assay mixture, containing membrane suspension (20 μg protein/tube) in 50 mM Tris-HCl buffer (pH 7.4), [^{3}H]diprenorphine, and various concentrations of test peptide, was incubated at room temperature for 1 h to allow binding to reach equilibrium. The samples were rapidly filtered through Whatman GF/C filters using a Brandel harvester (Brandel, Gaithersburg, MD, USA) and washed three times with 50 mM Tris-HCl buffer. The radioactivity retained on dried filters was determined by liquid scintillation counting after saturation with EcoLume liquid scintillation cocktail in a Wallac 1450 MicroBeta (Perkin-Elmer; Waltham). Nonspecific binding was determined using 10 μM naloxone. K_i values were calculated using nonlinear regression analysis to fit a logistic equation to the competition data using GRAPHPAD PRISM version 5.01 for Windows (GraphPad Software Inc., La Jolla, CA, USA). The results presented are the mean ± standard error from at least three separate assays performed in duplicate.

Stimulation of [^{35}S]GTPγS Binding

Agonist stimulation of [^{35}S] guanosine 5′-O-[gamma-thio]triphosphate ([^{35}S]GTPγS, 1250 Ci, 46.2TBq/mmol) binding was measured as described previously (29). Briefly, membranes (10–20 μg of protein/tube) were incubated 1 h at room temperature in GTPγS buffer (50 mM Tris-HCl, 100 mM NaCl, 5 mM $MgCl_2$, pH 7.4) containing 0.1 nM [^{35}S]GTPγS, 100 μM guanosine diphosphate (GDP), and varying concentrations of test peptides. Peptide stimulation of [^{35}S]GTPγS was compared with 10 μM standard compounds [D-Ala^2, N-MePhe^4, Gly-ol]-enkephalin (DAMGO) at MOR, D-Pen^{2,5}- enkephalin (DPDPE) at DOR, or U69,593 at KOR. The reaction was terminated by rapidly filtering through GF/C filters and washing ten times with GTPγS buffer, and retained radioactivity was measured as described earlier. The results presented are the mean ± standard error from at least three separate assays performed in duplicate; maximal stimulation was determined using nonlinear regression analysis with GRAPHPAD PRISM.

Determination of K_e through stimulation of [^{35}S]GTPγS Binding

Agonist stimulation of [^{35}S] guanosine 5′-O-[gamma-thio]triphosphate ([^{35}S]GTPγS, 1250 Ci, 46.2TBq/mmol) binding was measured for known agonists, [D-Ala^2, N-MePhe^4, Gly-ol]-enkephalin (DAMGO) at MOR and D-Pen^{2,5}- enkephalin (DPDPE) at DOR, as described earlier. Control wells contained only membranes (10–20 μg of protein/tube) GTPγS buffer (50 mM Tris-HCl, 100 mM NaCl, 5 mM $MgCl_2$, pH 7.4) containing 0.1 nM [^{35}S]GTPγS, 100 μM guanosine diphosphate (GDP), and varying concentrations of known agonists. Test wells contained all of the same components as the control wells, as well as a constant concentration of the test antagonist. The assay mixture was incubated for 1 h at room temperature and was terminated by rapidly filtering through GF/C filters and washing ten times with GTPγS buffer. Retained radioactivity was measured as described earlier. The results presented are the mean ± standard error from at least three separate assays performed in duplicate; EC_{50} values were determined using nonlinear regression analysis with GRAPHPAD PRISM and K_e values calculated based of these EC_{50} values.

Receptor modeling

The homology modeling of opioid receptors in complexes with peptide ligands was performed as previously described (6,8,19,30). The procedure included the following steps: (i) residue substitution in corresponding structural template(s); (ii) rigid body helix movement to reproduce structural rearrangement during receptor activation observed in crystal structures of rhodopsin and adrenergic receptor (31); (iii) peptide ligand docking in accordance with mutagenesis-derived constraints; and (iv) refinement of receptor–ligand complex using distance geometry and energy minimization with CHARMm. The validity of this modeling procedure has been assessed in blind prediction experiments of structural modeling of MOR (6,8), A_{2a}-adenosine receptor (32), CXCR4, and D3 dopamine receptor (30)

performed before the release of the corresponding crystal structures. The following comparison with experimental structures showed relatively high accuracy of our homology models: rmsd were between 1.5 and 2.5 Å for seven transmembrane helices (30,32). A comparison of our previously developed opioid receptor models (6,8,24,33) and recently released crystal structures of the mouse MOR (34) and the human KOR (35) demonstrated the high reliability in prediction of ligand–receptor interactions in the more conserved 'message' region located deeply in the ligand binding pocket, and less precise modeling in the 'address' region of flexible extracellular loops, which are responsible for ligand selectivity. Despite some inaccuracies, the previous models suggested the important role of interactions between Met^{199} and Trp^{284} of DOR and pentapeptide Phe^3 and Phe^4 side chains, respectively, and aromatic interactions between pentapeptide Phe^4 side chain and residues from the extracellular loop 2 (6,7,24,33).

For this study, we used X-ray structures of the mouse MOR (PDB ID: 4dkl) and the human KOR (PDB ID: 4djh) as inactive receptor conformations for docking peptide ligands in a mode similar to that of co-crystalized antagonists. To minimize steric hindrances, manual docking of peptides in low-energy conformations was followed by the automated rigid docking implemented in QUANTA (Accelrys Inc). The MOR crystal structure was also used to generate the homology model of the inactive conformation of the human DOR (UniProt ID: P41143, residues 46–333). The comparison of this DOR model with the experimental structure of the mouse DOR (PDB ID: 4ej4) (36) released after manuscript submission demonstrates their close resemblance (rmsd 1.16 Å for 249 Cα-atoms) in all regions except some parts of extracellular loops 2 and 3 (residues 192–195, 288–295). In the experimental DOR, structure residues Asp^{290}–Arg^{291} of the extracellular loop 3 appear to be located deeper in the binding pocket than we anticipated, thus forming additional contacts with the variable 'address' region of peptides. However, the shift of this loop does not alter essential interactions between the common 'message' region of cyclic peptides and receptor residues, which has been previously suggested based on our and other mutagenesis data (18,19). These interactions included hydrogen-bonding between peptide N^+ and Asp from TM3 (Asp^{128} in DOR), water-mediated hydrogen-bonding between OH-group of peptide Tyr^1 and His from TM6 (His^{278} in DOR), aromatic interactions between Tyr^1 of peptide and Tyr from TM3 (Tyr^{129} in DOR), and interactions of the disulfide bridge of the peptide with TM6 (Val^{281} in DOR).

Further, we used the crystal structure of the human KOR (PDB ID: 4djh) together with our previous active state models (6,8) for modeling of the active conformations of the mouse MOR using the procedure described earlier. The KOR structure was chosen as a modeling template because it demonstrates some inward movement of the extracellular ends of TMs 2, 5, 6, and 7 and the outward shift of TM3, as compared to other opioid receptor structures (PDB IDs: 4dkl, 4ej4). Similar helix movements were attributed to the activated receptor conformation (31). However, although the experimental KOR structure shows some active-like rearrangements in the extracellular region, it does not reproduce the main characteristic feature of the activated receptors in the intracellular part – the TM6 rotation and the large shift of its N-terminus away from TM3 and closer to TM5 along with the shift of the end of TM7 toward TM2 (31). To reproduce these large relocations of intracellular ends of TMs 5, 6, and 7 associated with receptor activation, we used constraints from our previous models of the active receptor conformations (6,8). The thus obtained model of the activated MOR after energy refinement was used as a template for modeling of the active states of KOR and DOR using residue substitution followed by energy minimization. These models of the opioid receptor active conformations were used for docking high efficacy peptide ligands. Low-energy conformations of cyclic pentapeptides were generated using previously developed pharmacophore models of tetrapeptides (37) with additional conformational search in the region of the fifth residue and disulfide bridge. Co-ordinates of MOR (active and inactive states), DOR (inactive state), and KOR (active state) with peptide **1** can be downloaded from our website (http://mosberglab.phar.umich.edu/resources/).

Results and Discussion

To understand the basis for the relatively high KOR binding affinity of **1** and related compounds in the series (19), we docked **1** to our previously developed active state model of KOR (24,33). The docking suggested an important role of Phe^4 of peptide **1** in interacting with KOR. An improved active state model generated from the recently released crystal structure of KOR (35) demonstrates that Phe^4 of **1** indeed can form π-stacking interactions with Tyr^{219} from extracellular loop 2 located at the beginning of helix 5 (Figure 1). These interactions likely contribute to the binding and agonist character of peptide **1**. DOR and MOR lack a corresponding aromatic residue in the binding site – DOR has a Ser^{206} and MOR has a Thr^{225} in the analogous position. We hypothesized that changing the Phe^4 of peptide **1** to a nonaromatic residue would eliminate this favorable aromatic interaction with Tyr^{219} and thus decrease affinity to KOR. As shown in Table 1, replacing Phe^4 of peptide **1** with the aliphatic residues Leu, Ile, or Nle, in peptides **2** through **4** resulted in the predicted decreased binding to KOR (Table 1).

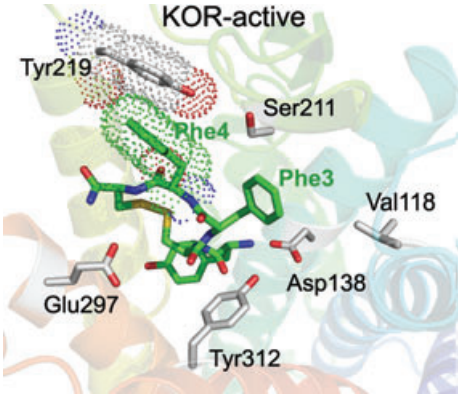

Figure 1: Modeling of peptide **1** (Tyr-c(S-S)[DCys-Phe-Phe-Cys]NH_2) docked in the KOR active state model. Highlighted is the π–π interaction between Phe^4 of **1** with Tyr^{219} of KOR (shown by dots). This favorable interaction appears to contribute to the high affinity of **1** for KOR as well as its agonist character.

As all three analogs with an aliphatic residue in position 4 displayed similar opioid profiles, high affinity and efficacy for MOR and DOR with low KOR activity, for convenience, we chose to carry forward with analogs containing the Nle[4] substitution. Because cyclic opioid pentapeptides with either D- or L-stereochemistry in residue 5 displayed similar MOR and DOR affinities in the initial examples of this series (19), we also examined the opioid profile of **5**, the D-Cys[5] diastereomer of **4**. This analog displayed a similar binding profile as **4**, but with somewhat reduced efficacy at both MOR and DOR (Table 1). Thus, we chose both **4** and **5** as starting points for modifications to reduce DOR efficacy.

To achieve this, we again relied on our previously described receptor models (6,8,20–24), which suggested that bulkier aromatic side chains replacing Phe[3] or Phe[4] of the ligands would better fit the large and more open antagonist binding pocket of the receptors in the inactive state, while having steric clashes in the more narrow agonist binding pocket of the active receptor conformation. A greater effect was expected for DOR, which has more bulky residues, Lys[108], Met[199], and Trp[284], occluding the ligand binding pocket than MOR, with Asn[127], Thr[218], and Lys[303] at the corresponding positions. Examination of our current, refined models of DOR and MOR in complex with **1** supported our previous suggestions (Figure 2). Of particular importance, here is the observation that Phe[3] of peptide **1** is in close proximity to Met[199] in the DOR agonist binding pocket (Figure 2A). However, in the DOR antagonist binding site (Figure 2B), Met[199] is angled away from the ligand, enlarging the binding pocket. Replacing the Phe[3] of peptide **1** with a larger residue would be expected to increase the steric clash between the ligand and the active conformation of DOR, disfavoring the binding of the ligand to the active conformation and thus reducing its agonist efficacy, as we have observed before (8). However, because of the presence of the smaller side chain of Thr[218] in the MOR binding pocket (Figure 2C) instead of Met[199] in the DOR binding pocket, adding steric bulk in the 3 position of peptide **1** should have less effect on MOR efficacy. Consequently, we prepared and pharmacologically assessed a series of pentapeptides based on **4** and **5**, in which the Phe[3] residue was replaced by 1-Nal or 2-Nal (Table 2).

Peptides **6**–**9** represent the 1-Nal[3] and 2-Nal[3] analogs of **4** and **5**. As seen in Table 2, replacing the Phe[3] of **4** or **5** with 2-Nal (analogs **6** and **7**, respectively) greatly reduces efficacy at both MOR and DOR, consistent with our earlier observations (6), while also greatly reducing affinity at DOR. By contrast, the 1-Nal[3] analogs **8** and **9** display a more promising profile in which DOR efficacy is more selectively affected and DOR affinity is less drastically reduced. In analogs **6**–**9,** the D-Cys[5] diastereomer exhibits a greater ability to reduce efficacy than the corresponding L-Cys[5], but this effect is equally expressed at MOR and DOR.

In compounds **10** and **11,** we examined the effect of increasing the ring size of the 14-membered disulfide scaffold of **8** and **9** to a 16-membered ethylene dithioether-containing cycle, an approach we have often used to modulate opioid activity (6,19,33). In the present case, increasing the cycle size had little effect on binding affinity or efficacy, with the exception of a rather large reduction in maximal stimulation at MOR (51% versus 100% stimulation relative to the standard, DAMGO) and a slight increase in KOR affinity displayed by **10** compared to **8**.

Among peptides **6**–**11,** the most promising is **8** that possesses high MOR affinity, full agonist behavior at MOR and greatly reduced DOR efficacy (22% of DOR standard DPDPE). However, **8** displays ~18-fold lower affinity at DOR compared with MOR. Furthermore,

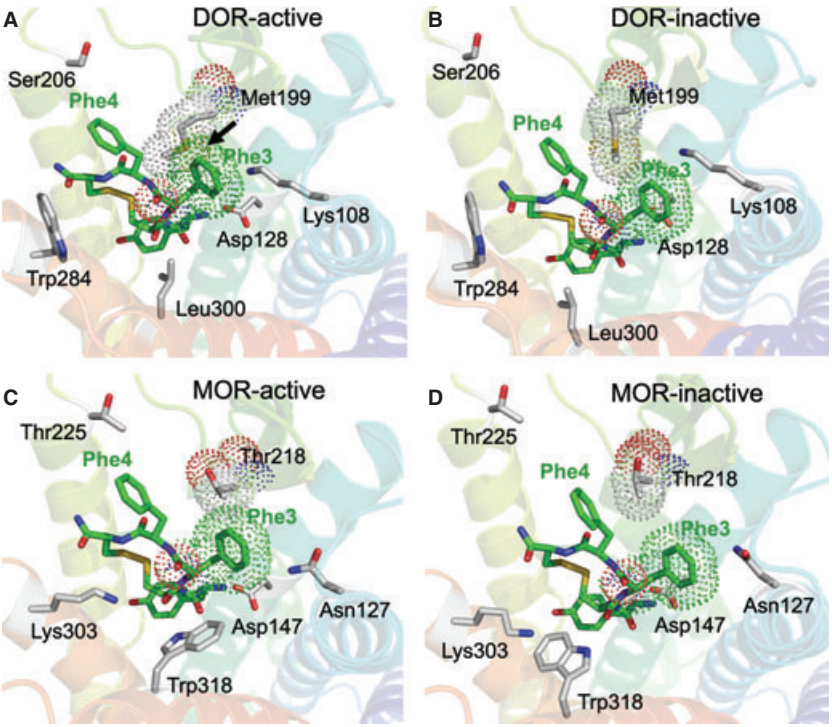

Figure 2: Modeling of peptide **1** (Tyr-c(S-S)[DCys-Phe-Phe-Cys]NH_2) docked in the active and inactive state models of DOR (A and B) and MOR (C and D). Docking of **1** to the active state of DOR shows a steric clash between Phe[3] of **1** and Met[199] of DOR, highlighted by an arrow in 2A; this steric clash is not seen when **1** is docked in the DOR inactive state binding site or the MOR active or inactive state binding sites.

Table 2: Binding Affinities and Efficacies of Peptides **6**–**15**

Peptide	Sequence	K_i (nM)			Efficacy % standard			
		MOR	DOR	KOR	MOR	MOR EC_{50} (nM)	DOR	KOR
6	Tyr-c(S-S)[DCys-2Nal-Nle-Cys]NH_2	2.4 ± 1.3	240 ± 70	1000 ± 420	25 ± 1		32 ± 11	dns
7	Tyr-c(S-S)[DCys-2Nal-Nle-DCys]NH_2	2.1 ± 0.9	950 ± 190	1400 ± 500	9.3 ± 0.9		dns	dns
8	Tyr-c(S-S)[DCys-1Nal-Nle-Cys]NH_2	0.65 ± 0.3	12 ± 2.7	730 ± 330	100 ± 2	5.1 ± 1.4	22 ± 0.9	<7
9	Tyr-c(S-S) [DCys-1Nal-Nle-DCys]NH_2	1.4 ± 0.3	56 ± 2.5	1200 ± 350	43 ± 2.7	17.5 ± 5.0	dns	<5
10	Tyr-c(S-$(CH_2)_2$-S)[DCys-1Nal-Nle-Cys]NH_2	1.3 ± 0.1	37 ± 1.5	180 ± 90	51 ± 6	8.3 ± 1.3	24 ± 1	<7
11	Tyr-c(S-$(CH_2)_2$-S) [DCys-1Nal-Nle-DCys]NH_2	1.4 ± 0.4	23 ± 2.9	770 ± 140	31 ± 1.2		dns	<7
12	Tyr-c(S-S) [DCys-1Nal-Nle-Cys]OH	3.7 ± 2	11 ± 3	5100 ± 2600	94 ± 1	3.4 ± 0.8	17 ± 2	30 ± 8
13	Tyr-c(S-S) [DCys-1Nal-Nle-DCys]OH	2.7 ± 0.3	4.0 ± 0.5	5600 ± 500	dns		dns	dns
14	Tyr-c(S-$(CH_2)_2$-S) [DCys-1Nal-Nle-Cys]OH	8.6 ± 1.4	58 ± 8.3	1300 ± 100	47 ± 4	35.5 ± 5.0	11 ± 8	nt
15	Tyr-c(S-$(CH_2)_2$-S) [DCys-1Nal-Nle-DCys]OH	3.1 ± 0.04	29 ± 4	1000 ± 200	39 ± 3.4		7.3 ± 1.4	nt

Binding affinities (K_i) were obtained by competitive displacement of radiolabeled [^{3}H] diprenorphine. Efficacy data were obtained using [^{35}S] GTPγS binding assay. Efficacy is represented as per cent maximal stimulation relative to standard agonists DAMGO (MOR), DPDPE (DOR), or U69,593 (KOR) at 10 μM concentrations. EC50 values are provided for compounds displaying >40% maximal stimulation. All values are expressed as mean ± SEM of three separate assays performed in duplicate. Cyclization abbreviated as S-S for disulfide linkage and S-$(CH_2)_2$-S for ethylene dithioether, nt = not tested, dns = does not stimulate.

8 lacks the undesired KOR activity, which make it a promising ligand for the exploration of functional MOR/DOR interactions.

Peptides **12**–**15**, the C-terminal carboxylic acid counterparts of the carboxamide terminal **8**–**11**, were designed to restore a balance in MOR and DOR affinity, because negatively charged C-terminal groups often interfere with MOR binding (38). As seen in Table 2, the carboxy-terminal analogs displayed the expected decrease in MOR affinity, decreased KOR affinity, but little significant effect on DOR binding. Peptide **13** was an exception, in that DOR affinity improved approximately 13-fold compared with **9** (K_i = 4 versus 56 nM). Both disulfide-containing C-terminal carboxylic acids, **12** and **13**, display the desired binding profile: high affinity for MOR and DOR, low affinity for KOR. The dithioether-containing analogs, **14** and **15,** have less desirable binding profiles displaying somewhat lower and/or less balanced MOR and DOR affinity and reduced MOR efficacy.

Examination of the efficacy profiles of **12** and **13** reveals an interesting observation. While **12**, like its carboxamide terminal counterpart **8**, is a full agonist at MOR, with low partial DOR agonism (~20% maximal stimulation versus DPDPE), peptide **13**, which differs from **12** only in the stereochemistry of the C-terminal Cys, acts as an antagonist at both MOR and DOR. The functional antagonist properties of **13** were confirmed by examining its effect on stimulation of GTPγS binding of MOR by DAMGO and of DOR by DPDPE. In both cases, 13 shifted the dose–response curve of the standard ligand with K_e values of 2.13 ± 0.64 and 20.3 ± 6.3 nM for DAMGO and DPDPE, respectively. Reduced efficacy of D-Cys^5 versus L-Cys^5-containing analogs is a consistent feature among the compounds shown in Table 2; however, the complete elimination of MOR efficacy for **13** was unexpected. An explanation for this behavior can be deduced from examination of **12** and **13** docked to the active and inactive states of MOR. Figure 3A depicts **12** bound to our model of the MOR active receptor. In this model, the C-terminal COO- of **12**, while being close to Glu^{229} from transmembrane helix 5, may also form an ionic bridge with the positively charged side chain of Lys^{303} from helix 6. This ionic bridge can be formed only in MOR and only in the active conformation, but not in DOR or KOR, which have Trp^{284} (DOR) or Glu^{297} (KOR) in the corresponding position in helix 6. The favorable ionic interactions of **12** in the agonist binding pocket of MOR may explain its behavior as an efficacious MOR agonist. The unfavorable ionic interaction between the C-terminal carboxylate of **12** and Glu^{229} from helix 5 in MOR or Glu^{297} from helix 6 in KOR is consistent with the six and sevenfold decreased affinity of **12** to MOR and KOR, respectively, as compared to **8** with a C-terminal amide. For **13**, the change in stereochemistry of residue 5 orients the terminal COO- away from Lys^{303} and toward Glu^{229}, resulting in an unfavorable ionic repulsion. However, in the inactive conformation of MOR (Figure 3B), rotation of Glu^{229} and Lys^{233} relieves this repulsion. In the DOR models, the C-terminus of **13** is close to the Asp^{210}–Lys^{214} pair from helix 5 and can form favorable ionic interactions with Lys^{214} in the inactive receptor conformation. These ligand–receptor interactions help explain the antagonist activity of **13** in MOR and its improved binding and antagonist activity at DOR.

Conclusions

The studies discussed in this article were aimed toward developing opioid ligands that display high affinity and efficacy for MOR, high affinity and low efficacy for DOR and low affinity for KOR. Using our validated receptor models of the active and inactive states of all three receptors for structure-based design, we were able to achieve this goal by selectively modulating the affinity and efficacy of our lead peptide **1**. First, examination of docking of the lead peptide, **1**, to active state KOR suggested the participation of the ligand's Phe^4 residue in an aromatic π–π interaction unavailable in MOR or DOR. Replacement of this Phe^4 with an aliphatic residue (peptides **2**–**4**) achieved the desired result of greatly reducing KOR affinity and efficacy. Next, predicted differences in ligand docking to the DOR active and inactive conformations were exploited by incorporating bulkier residues in the third position of peptide **1** to favor binding to the DOR inactive conformation. As predicted, the use of 1-Nal or 2-Nal in place of Phe^3 greatly reduced DOR

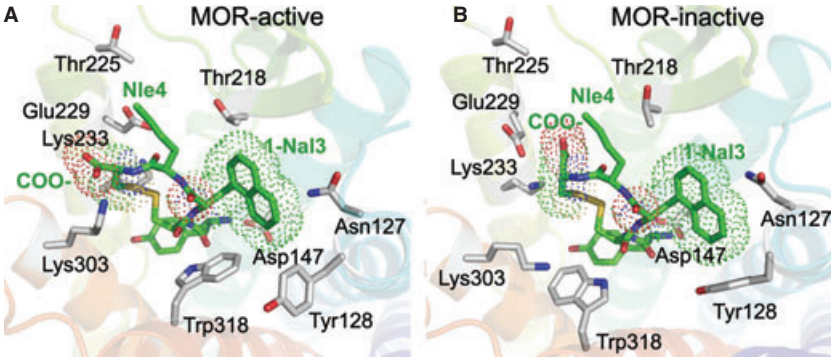

Figure 3: Modeling of peptide **12** (Tyr-c(S-S)[DCys-1Nal-Nle-Cys]OH) docked in the active state model of MOR (A) and **13** (Tyr-c(S-S)[DCys-1Nal-Nle-DCys]OH) docked in the inactive state model of MOR (B). The C-terminal COO- of **12** forms a favorable ionic interaction with Lys^{303}. However, when **13** is docked in the active site, the C-terminal COO- is angled toward Glu^{229}, resulting in an unfavorable repulsion (not shown); in the inactive state, rotation of Glu^{229} and Lys^{233} relieves this repulsion and allows a favorable interaction with Lys^{233}.

efficacy. Analogs **8** and **12**, in particular, with 1-Nal^3, exhibited the desired profile of high MOR/low DOR efficacy. The wide range of affinity and efficacy shown by the closely related analogs in Table 2 reflects both the structural sensitivity of the ligand–receptor interaction and the utility of peptides, whose structures can be easily and subtly manipulated for probing the details of the ligand–receptor interaction. Of particular note is the profound functional difference observed for **12** and **13**, which differ only in stereochemistry of the C-terminal residue and which possess similar affinity, but quite different efficacy profiles. The results reported here further validate our receptor models and our approach of using these models for rational design to exploit differences in the opioid receptors highly homologous binding pockets.

Acknowledgments

We would like to thank Katarzyna Sobczyk-Kojiro for her assistance with the synthesis of precursors to peptides **13** and **15**. This work was funded by NIH grants DA004087 (J.R.T.) and DA003910 (H.I.M.). J.P.A. was supported by NIH training grants DA007281 and GM007767. L.C.P. was supported by NIH training grant DA007267.

References

1. Morphy R., Kay C., Rankovic Z. (2004) From magic bullets to designed multiple ligands. Res Focus Rev;9:641–652.
2. Morphy R., Rankovic Z. (2009) Designing multiple ligands – medicinal chemistry strategies and challenges. Curr Pharm Des;15:587–600.
3. Abdelhamid E.E., Sultana M., Portoghese P.S., Takemori A.E. (1991) Selective blockage of the delta opioid receptors prevents the development of morphine tolerance and dependence in mice. J Pharmacol Exp Ther;258:299–303.
4. Fundytus M.E., Schiller P.W., Shapiro M., Weltrowska H., Coderre T.J. (1995) Attenuation of morphine tolerance and dependence with the highly selective delta opioid receptor antagonist TIPP(psi). Eur J Pharmacol;286:105–108.
5. Hepburn M.J., Little P.J., Gringas J., Khun C.M. (1997) Differential effects of naltrindole on morphine-induced tolerance and physical dependence in rate. J Pharmacol Exp Ther;281:1350–1356.
6. Purington L.C., Pohozheva I.D., Traynor J.R., Mosberg H.I. (2009) Pentapeptides displaying mu opioid receptor agonist and delta opioid receptor partial agonist/antagonist properties. J Med Chem;52:7724–7731.
7. Schiller P.W. (2009) Bi- or multifunctional opioid peptide drugs. Life Sci;86:598–603.
8. Purington L.C., Sobczyk-Kojiro K., Pogozheva I.D., Traynor J.R., Mosberg H.I. (2011) Development and in vitro characterization of a novel bifunctional mu-agonist/delta-antagonist opioid tetrapeptide. J Chem Biol;6:1375–1381.
9. Anathan S., Kezar H.S., Carter R.L., Saini S.K., Rice K.C., Wells J.L., Davis P., Xu H., Dersch C.M., Bilsky E.J., Porreca F., Rothman R.B. (1999) Synthesis, opioid receptor binding, and biological activities of naltrexone-derived pyrido- and pyrimidomorphans. J Med Chem;42:3527–3538.
10. Anathan S., Khare N.K., Saini S.K., Seitz L.E., Bartlett J.L., Davis P., Davis P., Xu H., Dersch C.M., Bilsky E.J., Porreca F., Rothman R.B. (2004) Identification of opioid ligands possessing mixed mu agonist/delta antagonist activity among pyridomorphans derived from naloxone, oxymorphone, and hydromorphone. J Med Chem;47:1400–1412.
11. Balboni G., Guerrini R., Salvadori S., Bianchi C., Rizzi D., Bryant S.D. *et al.* (2002) Evaluation of the Dmt-Tic pharmacophore: conversion of a potent delta-opioid receptor antagonist into a potent delta agonist and ligands with mixed properties. J Med Chem;45:713–720.
12. Balboni G., Salvadori S., Guerrini R., Negri L., Giannini E., Jinsmaa Y. *et al.* (2002) Potent delta-opioid receptor agonists containing the Dmt-Tic pharmacophore. J Med Chem;45:5556–5563.
13. Cheng K., Kim I.J., Lee M.J., Adah S.A., Raymond T.J., Bilsky E.J. *et al.* (2007) Opioid ligands with mixed properties from substituted enatiomeric *N*-phenethyl-5-phenylmorphans: synthesis of mu-agonist delta-antagonist and delta-inverse agonists. Org Biomol Chem;5:1177–1190.
14. Heibel A.C., Lee Y.S., Bilsky E.J., Guivelis D., Deschamps J.R., Parrish D. *et al.* (2005) Synthesis and structure-activity relation-

ships of a potent mu-agonist delta-antagonist and an exceedingly potent antinociceptive in the enantiomeric C9-substituted 5-(3-hydroxyphenyl)-*N*-phenylethylmorphan series. J Med Chem;50:3765–3776.
15. Salvadori S., Guerrini R., Balboni G., Bianchi C., Bryant S.D., Cooper P.S. *et al.* (1999) Further studies on the Dmt-Tic pharmacophore: hydrophobic substituents at the C-terminus endow delta antagonists to manifest mu agonism of mu antagonism. J Med Chem;42:5010–5019.
16. Yamamoto T., Nair P., Vagner J., Largent-Milnes T., Davis P., Ma S.W. *et al.* (2008) A structure-activity relationship study and combinatorial synthetic approach to C-terminal modified bifunctional peptides that are Delta/Mu Opioid receptor agonists and neurokinin 1 receptor antagonists. J Med Chem;51:1369–1376.
17. Schiller P.W., Fundytus M.E., Merovitz L., Weltrowska G., Nguten T.M.-D., Lemieux C. *et al.* (1999) The opioid mu agonist/delta antagonist DIPP-NH2(psi) produces a potent analgesic effect, no physical dependence and less tolerance than morphine in rate. J Med Chem;42:3520–3526.
18. Schmidt R., Vogel D., Mrestani-Klaus C., Brandt W., Neubert K., Chung N.N. *et al.* (1994) Cyclic beta-casomorphin analgoues with mixed mu agonist/delta antagonist properties: synthesis, pharmacological characterization and conformational aspects. J Med Chem;37:1136–1144.
19. Przydzial M.J., Pogozheva I.D., Ho J.C., Bosse K.E., Sawyer E., Traynor J.R. *et al.* (2005) Design of high affinity cyclic pentapeptide ligands for the kappa opioid receptors. J Pept Res;66:255–262.
20. Fowler C.B., Pogozheva I.D., Lomize A.L., LeVine H., Mosberg H.I. (2004) Refinement of a homology model of the Mu-opioid receptor using distance constraints from Intrinsic and engineered zinc-binding sites. Biochemistry;43:8700–8710.
21. Fowler C.B., Pogozheva I.D., Lomize A.L., LeVine H., Mosberg H.I. (2004) Complex of an active Mu-opioid receptor with a cyclic peptide agonist modeled from experimental constraints. Biochemistry;43:15796–15810.
22. Pogozheva I.D., Lomize A.L., Mosberg H.I. (1997) The transmembrane 7-alpha-bundle of Rhodopsin: distance geometry calculations with hydrogen bonding constraints. Biophysics;72:1963–1985.
23. Pogozheva I.D., Lomize A.L., Mosberg H.I. (1998) Opioid receptor three-dimensional structures from distance geometry calculations with hydrogen bonding constraints. Biophysics;75:612–634.
24. Pogozheva I.D., Przydzial M.J., Mosberg H.I. (2005) Homology modeling of opioid receptor-ligand complexes using experimental constraints. AAPS Journal;7:43–57.
25. Pfeiffer A., Brantl V., Herz A., Emrich H.M. (1986) Psychotomimesis mediated by kappa opioid receptors. Science;233:774–776.
26. Przydzial M.J., Pogozheva I.D., Andrews S.M., Tharp T.A., Traynor J.R., Mosberg H.I. (2005) Roles of residues 3 and 4 in cyclic tetrapeptide ligand recognition by the kappa opioid receptor. J Pept Res;26:333–342.
27. Lee K.O., Akil H., Woods J.H., Traynor J.R. (1999) Differential binding properties of oripavines at cloned mu- and delta-opioid receptors. Eur J Pharmacol;32:3–30.
28. Husbands S.M., Neilan C.L., Broadbear J., Grundt P., Breeden S., Aceto M.D. *et al.* (2005) BU74, a complex oripavine derivative with potent kappa opioid receptor agonism and delayed opioid antagonism. Eur J Pharmacol;11:7–35.
29. Traynor J.R., Nahorski S.R. (1995) Modulation by mu-opioid agonists of guanosine-5′-O(3-[35S]thio)triphosphate binding to membranes from human neuroblastoma SHY5Y cells. Mol Pharmacol;84:8–54.
30. Kufareva I., Rueda M., Katritch V., Stevens R.C., Abagyan R., participants G.D. (2011) Status of GPCR modeling and docking as reflected by community-wide GPCR Dock 2010 assesment. Structure;19:1108–1126.
31. Congreve M., Langmead C.J., Mason J.S., Marshall F.H. (2011) Progress in structure based drug design for G protein-coupled receptors. J Med Chem;54:4283–4311.
32. Michino M., Abola E., Participants G.D., Charles L.Brooks.I., Dixon J.S., Moult J. *et al.* (2008) Community-wide assesment of GPCR structure modeling and ligand docking. Nat Rev Drug Discov;8:455–463.
33. Mosberg H.I., Omnaas J.R., Smith C.B., Medzihradsky F. (1988) Cyclic disulfide and dithioether-containing opioid tetrapeptides: development of a ligand with enhanced delta opioid receptor selectivity and potency. Life Sci;43:1013–1020.
34. Manglik A., Kruse A.C., Kobilka T.S., Thian F.S., Mathiesin J.M., Sunahara R.K. *et al.* (2012) Crystal structure of the mu opioid receptor bound to a morphinan antagonist. Nature;485:321–326.
35. Wu H., Wacker D., Mileni M., Katritch V., Han G.W., Vardy E. *et al.* (2012) Structure of the human kappa opioid receptor in complex with JDTic. Nature;485:327–332.
36. Granier S., Manglik A., Kruse A.C., Kobilka T.S., Thian F.S., Weis W.I., Kobilka B.K. (2012) Structure of the δ-opioid receptor bound to naltrindole. Nature;485:400–404.
37. Lomize A.L., Flippen-Anderson J.L., George C., Mosberg H.I. (1994) Conformational analysis of the delta receptor selective cyclic opioid peptide Tyr-c[DCys-Phe-DPen]OH (JOM13). Comparison of X-ray cystallographic structures, molecular mechanics simulations, and 1H NMR data. J Am Chem Soc;116:429–436.
38. Mosberg H.I., Fowler C.B. (2002) Development and validation of opioid ligand-receptor interaction models: the structural basis of mu vs. delta selectivity. J Pept Res;60:329–335.